EXPLAINING AND FORECASTING INTERANNUAL VARIABILITY IN THE FLOW OF THE NILE RIVER

Mohamed S. Siam[1]

Ralph M. Parsons Laboratory, Massachusetts Institute of Technology, Cambridge, Massachusetts

Elfatih A. B. Eltahir

Ralph M. Parsons Laboratory, Massachusetts Institute of Technology, Cambridge, Massachusetts

[1]*Corresponding author address*: Mohamed Siam, Ralph M. Parsons Laboratory, Massachusetts Institute of Technology, 15 Vassar St. Cambridge, MA 02139.

E-mail:msiam@mit.edu

EXPLAINING AND FORECASTING INTERANNUAL VARIABILITY IN THE FLOW OF THE NILE RIVER

Abstract

This study analyzes extensive data sets collected during the 20th century and define four modes of natural variability in the flow of Nile River, identifying a new significant potential for improving predictability of floods and droughts. Previous studies have identified a significant teleconnection between the Nile flow and the Eastern Pacific Ocean. El Niño-Southern Oscillation (ENSO) explains about 25% of the interannual variability in the Nile flow. Here, this study identifies a region in the southern Indian Ocean with similarly strong teleconnection to the Nile flow. Sea Surface Temperature (SST) in the region (50^{o}E-80^{o}E and 25^{o}S-35^{o}S) explains 28% of the interannual variability in the Nile flow. During those years with anomalous SST conditions in both Oceans, this study estimates that indices of the SSTs in the Pacific and Indian Oceans can collectively explain up to 84% of the interannual variability in the flow of Nile. Building on these findings, this study uses classical Bayesian theorem to develop a new hybrid forecasting algorithm that predicts the Nile flow based on global models predictions of indices of the SST in the Eastern Pacific and Southern Indian Oceans.

1. Introduction

The Nile basin covers an area of 2.9 $x10^6$ km^2, which is approximately 10% of the African continent (Fig. 1). It has two main tributaries; the White Nile and the Blue Nile that originate from the equatorial lakes and Ethiopian highlands respectively. The Upper Blue Nile (UBN) basin is the main source of water for the Nile River. It contributes to approximately 60% of the annual flow of the Nile and 80% of the total Nile flow that occurs between July and October at Dongola (Conway and Hulme, 1993) (Fig. 2). The UBN basin extends over an area of 175 $x10^3$ km^2 (7° N to 12°5' N and from 34°5' E to 40° E). The mean annual rainfall over this basin is 1200 mm/year (Conway and Hulme, 1993). Almost 60% of the annual rainfall over the UBN occurs during the summer between July and August, resulting in a largely predictable seasonal variability in the flow of the river.

The predictability of inter-annual variability in the flow of the Nile is rather challenging. Many studies investigated the teleconnections between the Ethiopian rainfall and the global SSTs in order to find SSTs indices to use for Nile flow prediction (e.g. Eltahir, 1996; Abtew et al., 2009; and Melesse et al., 2011). Eltahir, 1996 showed that the SSTs anomalies over the tropical Eastern Pacific Ocean explains 25% of the inter-annual variability of Nile flow. ElSanabary et al., 2014 showed that the dominant frequencies of the Ethiopian rainfall ranged between 2 and 8 years and that the scale averaged wavelet power of the SSTs over the Eastern Pacific and South Indian and Atlantic Oceans can explain significant fraction of the rainfall variability over Ethiopia using wavelet principal component analysis. These correlations were the basis for new forecast models that were proposed to predict the Nile flows. For example, Wang and Eltahir (1999) used a discriminant prediction approach to estimate the probabilities that the Nile flow will fall into

prescribed categories. Eldaw et al., (2003) and Gissila et al., (2004) used sea surface temperature (SST) over the Pacific, Indian and Atlantic Oceans as predictors within a multiple linear regression model to predict the Nile flow.

The mechanisms behind these teleconnections between the rainfall over Ethiopia and the global SSTs were examined in several studies (e.g. Beltrando and Camperlin, 1993). However, a clear distinction must be made between rainfall over the UBN basin in Ethiopia and rainfall over East Africa, defined as the region along the coast, east of the Ethiopian highlands (Fig. 1). The UBN basin has one rainy season (May to September) during which more than 80% of the rainfall occurs, while along the East coast of Africa and depending on the location from the equator, the seasonal cycle of rainfall can have two rainy seasons (Black et al., 2003, Hastenrath et al., 2011). This pattern in the seasonal cycle of rainfall is related to the migration of the Inter-tropical Convergence Zone (ITCZ) across the equator. Camberlin, 1995 showed that the rainfall over East Africa, including the UBN basin, is strongly coupled with the dynamics of the Indian monsoon. During strong Indian monsoon seasons, the sea level pressure over India decreases significantly, which enhances the pressure gradient between East Africa and India. As a result, westerly winds increase over Eastern Africa, which advect moisture from the Congo basin to Ethiopia, Uganda and western Kenya. Giro et al., 2010 also showed that the warming over the Pacific Ocean, during El Niño events, reduces these westerly winds, which reduce the rainfall over East Africa. In addition, the monsoon circulation is weaker during El Niño events due to modulation of the walker circulation and enhanced subsidence over the Western Pacific and South Asia, thus the rainfall over Ethiopia decreases (Ju and Slingo, 1995; Kawamura, 1998; Shukla and Wallace, 1983; Soman and Slingo, 1997). The reduced Nile flows during El Niño events were also attributed to the enhanced tropical-

67 scale subsidence that suppresses rainfall, as a consequence of the increased upwelling over the
68 Eastern Pacific Ocean (Amarasekera et al., 1996).
69
70 The physical mechanism of the teleconnection between the Nile flow and SSTs of North and
71 Middle Indian Ocean and ENSO is described in another paper by the authors (Siam et al., 2014).
72 Nile flow is strongly modulated by ENSO through ocean currents. During El Niño events, the
73 warm water travels from the Pacific to the Indian Ocean through the "Indonesian through flow"
74 and advection by the Indian Equatorial Current (Tomczak and Godfrey, 1995). As a result, SSTs
75 in North and Middle Indian Ocean warm-up following the warming of Tropical Eastern Pacific,
76 and forces a Gill type circulation anomaly with enhanced westerly winds over Western Indian
77 Ocean (Yang et al., 2007). The latter enhances the low-level divergence of air and moisture away
78 from the Upper Blue Nile resulting in a reduction of rainfall over the basin. On the other hand, the
79 warming over the South Indian Ocean, generates a cyclonic flow in the boundary layer, which
80 reduces the cross-equatorial meridional transport of air and moisture towards the UBN basin,
81 favoring a reduction in rainfall and river flows. The tele-connections between the Pacific Ocean
82 and the Nile basin and between the Indian Ocean and the Nile basin are reflected in different modes
83 of observed natural variability in the flow of Nile River, with important implications for the
84 predictability of floods and droughts.
85
86 The objectives of the study are (i) to investigate the teleconnection between the Indian Ocean and
87 the Nile basin and its role in explaining observed natural modes of variability in the flow of the
88 Nile river, and (ii) to develop a new hybrid forecasting algorithm that can be used to predict the
89 Nile flow based on indices of the SST in the Eastern Pacific and Southern Indian Oceans.

2. Data

In this study we use observed SSTs over the Indian and Pacific oceans from the monthly global (HadISST V1.1) dataset on a 1 degree latitude-longitude grid from 1900 to 2000 (Rayner et al. 2003). The monthly flows at Dongola from 1900 to 2000 were extracted from the Global River Discharge Database (RivDIS v1.1) (Vörösmarty et al., 1998). The average monthly anomalies from September to November of the SSTs averaged over the Eastern Pacific Ocean (6^oN-2^oN, 170^oW-90^oW; 2^oN-6^oS, 180^oW-90^oW; and 6^oS-10^oS, 150^oW-110^oW) are used as an index of ENSO. This area has shown the highest correlation with the Nile flows and it is almost covering the same area as Niño 3 and 3.4 indices (Trenberth, 1997).

3. Relation between the variability in the flow of Nile river, ENSO and the Indian Ocean SST

Based on extensive correlation analysis of the Nile river flow at Dongola and the observed SST in the Indian Ocean, this study identifies a region over the Southern Indian Ocean (50^oE-80^oE and 25^oS-35^oS) (see Figure 3) as the one with the highest correlation between SST and the Nile flow. This correlation is especially high for river flow (accumulated for July, August, September and October) and SST during the month of August. In comparison to earlier studies, ElDaw et al. (2003) used SST indices over the Indian Ocean to predict the Nile flow, however, they focused on regions of the Indian Ocean that are different from the region that we use in defining the SIO index. In other words the region of the SIO was not used by ElDaw et al. (2003). Table 2 describes the regions of the Indian Ocean identified in both studies.

112 Here, this study emphasizes that the proposed forecasting methodology for the Nile flow is
113 motivated by the physical mechanisms proposed by Siam et al. (2014) and described in Section 1.
114 However, the forecasting approach of some of the previous studies was based on purely statistical
115 correlations found between the Nile flow and SSTs globally.

116

117 Figure 4 shows the observed and simulated time series of the average July to October Nile flow at
118 Dongola, which accounts for approximately 70% of the annual Nile flow. The Nile flow is
119 predicted by a linear regression model using ENSO averaged from September to November and
120 SIO August indices as predictors. It is clear from this figure that the addition of the SIO index
121 increase the explained variability of the Nile flow to 44%, compared to only 25% when ENSO
122 index is used alone. This indicates that the SIO index can explain almost 20% of the variability of
123 the Nile flow that is independent from ENSO. The North and middle of the Indian Ocean have
124 also exhibited a high correlation between their SST and the Nile flow. However, the additional
125 variability explained by the SST over the North and Middle Indian Ocean, when combined with
126 the ENSO index, is negligible (not shown here). This is mainly because the SSTs over the North
127 and Middle Indian Ocean are dependent on ENSO, while the SSTs over the South Indian Ocean
128 (i.e. SIO index) is not, as described in Section 1.

129

130 In further analysis, we define ±0.5^{o}C as the threshold between non-neutral and neutral years on the
131 Eastern Pacific Ocean based on ENSO index. This value is about two-thirds of one standard
132 deviation of the anomalies of ENSO index. The same threshold has been used to identify non-
133 neutral and neutral years using El Niño 3.4 index, which is similar to our ENSO index (Trenberth,

1997). This indicates that if the ENSO index anomaly is greater than 0.5^{o}C or less than -0.5^{o}C, it is considered as non-neutral condition, otherwise, it is considered as neutral condition. Similarly, ±0.3^{o}C value is used as a threshold between non-neutral and neutral years on the South Indian Ocean using the SIO index. This value is also about two-thirds of one standard deviation for the anomalies of the SSTs over this region. Thus, if both ENSO and SIO indices are used together, four different combinations can be defined based on these classifications. The first is when both ENSO and SIO indices are neutral (29 out of 100 events), the second is when both ENSO and SIO indices are non-neutral (19 out of 100 events), the third when SIO is non-neutral and ENSO is neutral (26 out of 100 events) and finally when SIO is neutral and ENSO is non-neutral (26 out of 100 events). Each of these combinations is considerate as a mode of natural variability in the flow of Nile river. Then the Nile flow is calculated as a predictant using multiple linear regression with the (ENSO and SIO indices) of each mode as predictors.

Four different modes are identified for describing the natural variability in the flow of Nile River and summarized in (Table 1). The ENSO and SIO indices do not explain a significant fraction of the interannual variability in the flow of river when they are both neutral (Fig. 5a). The variability of the Nile flow in such years can be regarded as a reflection of the chaotic interactions between the biosphere and atmosphere and within each of the two domains. For this mode, the predictability of the Nile flow is rather limited. The other two intermediate modes include non-neutral conditions in the Eastern Pacific and neutral conditions in the Southern Indian Oceans or vice versa (Fig. 5b and 5c). For these two modes, a significant fraction (i.e. 31% and 43%) of the variance describing inter-annual variability in the flow is explained. Hence, these modes point to a significant potential for predictability of the flow. Finally, indices of ENSO and SIO can explain 84% of the interannual

157 variability in the Nile flow when non-neutral conditions are observed for both the Eastern Pacific
158 and Southern Indian Oceans (Fig. 5d). Therefore, the SIO index can be used to predict the flow
159 together with the ENSO index, as collectively they can explain a significant fraction of the
160 variability in the flow of Nile River. This result indicates that during years with anomalous SST
161 conditions in both oceans, floods and droughts in the Nile River flow can be highly predictable,
162 assuming accurate forecasts of those indices are available.

163

164 **4. A Hybrid Methodology for Long-range Prediction of the Nile flow**

165 A simple methodology is proposed to predict the Nile flow with a lead time of about a few months
166 (~3-6 months). The forecast of global SST distribution based on dynamical models (e.g. NCEP
167 coupled forecast system model version 2 (CFSv2), Saha et al., 2010; Saha et al., under review),
168 can be used together with the algorithm developed in this section to relate the Nile flow to ENSO
169 and SIO indices. The proposed method is shown in Figure 6 and can be described in two main
170 steps:

171 • Forecast of SST anomalies in the Indian Ocean and Eastern Pacific Ocean using dynamical
172 models of the coupled global ocean atmosphere system. Such forecasts are routinely issued by
173 centers such NCEP and ECMWF.

174 • Application of a forecast algorithm between the Nile flow (predictand) and forecasted SSTs
175 in the Indian and Eastern Pacific Oceans (predictors) for the identified mode of variability.

176

177 In this paper we focus on the second step of the proposed method: the development of the algorithm
178 relating SSTs and the Nile flow. We develop the forecast algorithm using observed SSTs. We do
179 not describe how this algorithm can be applied with forecasts of global SST distribution based on
180 dynamical models as this step is beyond the scope of this paper. However, we recognize that
181 overall accuracy of this method in predicting interannual variability of the Nile flow is dependent
182 on the skill of global coupled models in forecasting the global SSTs (See Appendix for information
183 about forecasting models). Thus, the selection of the forecast model, which predicts the SSTs is
184 an important step to ensure the accuracy of the prediction of the Nile flow. As global coupled
185 ocean-atmosphere models improve in their skill of forecasting global SSTs in the Pacific and
186 Indian Oceans, we expect that our ability to predict the interannual variability in the Nile flow will
187 improve too. In addition, the accuracy in the prediction of the Nile flow at medium and short time
188 scales (of weeks to one month) can be improved by adding other hydrological variables (e.g.
189 rainfall and stream flow) over the basin, as demonstrated by (Wang and Eltahir, 1999)

190 The proposed method can be described as hybrid since it combines dynamical forecasts of global
191 SSTs, and statistical algorithms relating the Nile flow and the forecasted SSTs. The same method
192 can also be described as hybrid since it combines information about SSTs from the Pacific and the
193 Indian Oceans.

194 Here, we apply a discriminant approach that specifies the categoric probabilities of the predictand
195 (Nile flow) according to the categories that the predictors (i.e. ENSO and SIO indices) fall into.
196 The annual Nile flow is divided into “low”, “normal”, and “high” categories. The boundaries of
197 these categories are defined so that the number of points in each category is about a third of the
198 data points (Fig 7). On the other hand, the ENSO and SIO indices are divided into “cold”, “normal”
199 and “warm” categories. (The words Normal and Neutral are used to describe the same

conditions).The boundaries for the normal category are -0.5°C and 0.5°C for ENSO index and -0.3°C and 0.3°C for SIO index (Fig. 7). Any condition below the lower limit is considered "cold" and higher than the upper limit is considered "warm" for both indices.

The Bayesian theorem, described in many statistical books (e.g., Winkler 1972; West 1989), states that the probability of occurrence of a specified flow category (Q_i) and given two conditions (A and B) can be expressed as

$$P(Q_i/\ A,B)\ = \frac{P(B/Q_i,A)P(Q_i/A)}{P(B/A)} \qquad (1)$$

Where $P(Q_i/\ A)$ is the probability of event Q_i given that event A has occurred, and $P(Q_i/\ A,B)$ is the probability of event Q_i given that events A and B have occurred, and similarly for other shown probabilities. In addition, if the events A and B are independent, we can rewrite Eq. (1) as

$$P(Q_i/\ A,B)\ = \frac{P(B/Q_i)P(Q_i/A)}{\sum_{i=1}^{3} P(B/Q_i)P(Q_i/A)} \qquad (2)$$

The advantage of assuming independence between (A and B) and using Eq. (2), it simplifies the calculation of P(B/Q_i, A) since we do not have to split the data into a relatively large number of categories, which reduces the error due to the limitation of the data size. The independence between ENSO and SIO indices is a reasonable assumption as the coefficient of determination between them is less than 6%.

In order to evaluate the predictions of the Nile flow, we use a forecasting index (FI) defined by Wang and Eltahir, (1999) as

$$\text{FP(j)}= \sum_{i=1}^{3} P_r(i,j)\ P_p(i,j) \quad (3)$$

$$FI = \frac{1}{n}\sum_{i=1}^{n} FP\ (j) \qquad (4)$$

Where FP(j) is the forecast probability in a certain year (j) and the FI is the average of the FP over a certain period, n. The prior probability $P_r(i, j)$ is calculated using Eq.(2) for a certain year (j) and category (i=1, 2, 3) and the posterior probability $P_p(i, j)$ is defined as [1,0,0] in low flow year, [0,1,0] in normal year, and [0,0,1] in a high flow year. Hence, a larger FI indicates a higher accuracy of the forecast. The FI without any information about SST, should be about one third as we have classified flow data into three categories each with a similar number of the data points.

The data is split into a calibration period (1900-1970) and a verification period (1970-2000). Tables 3 and 4 summarize the conditional probabilities of Nile flow given certain conditions of SIO or ENSO index. It is shown that during "warm" and "cold" conditions of SIO, the probabilities are significantly higher for "low" and "high" Nile flow, respectively. The same is true for the ENSO, as was described originally by Eltahir (1996). Table 5 shows the probabilities that are conditioned on both SIO and ENSO, calculated using Eq. (2). This table illustrates clearly how forecasts of the Nile flow can be improved by combining the two indices. For example, "warm" conditions in both oceans translate into 85% probability of "low" flow in the Nile, and insignificant probability of "high" flow. On the other hand, "cold" conditions in both oceans translate into 83% probability of "high" flow in the Nile, and insignificant probability of "low" flow. Depending on the accuracy of the dynamical forecast models of global SSTs, such forecast of the Nile flow can be issued with lead times of 6 months. At present, the Eastern Nile Regional technical Office (ENTRO) issues operational forecasts of the Nile flow based on ENSO forecasts and the probability table described by Eltahir (1996) (similar to Table 4). We anticipate that use of Table 5, would represent a significant improvement in these operational forecasts.

The combined use of ENSO and the SIO indices significantly increased the FI to 0.5 (Figure 8a). Comparison of Figures 8b and 8c, illustrates that the SIO index alone has almost the same FI value as ENSO index. Recall that in absence of any information about global SSTs, the FI should have a value of one third. The deviations of the FI using ENSO index alone (Figure 8b) or SIO index alone (Figure 8c) from one third are almost added together to create the deviation of the FI from the hybrid method from one third (Figure 8a). Hence, the new SIO index plays an independent role from ENSO in shaping the interannual variability in the flow of Nile River. Thus by using these two indices, we explain a significant fraction of the interannual variability in the flow of Nile River, and illustrate a significant potential for improving the Nile flow forecasts.

5. Conclusions

- In this paper, we document that the SSTs in the Eastern Pacific and Indian Oceans play a significant role in shaping the natural interannual variability in the flow of Nile River. Previous studies have identified a significant teleconnection between the Nile flow and the Eastern Pacific Ocean. El Niño-Southern Oscillation (ENSO) explains about 25% of the interannual variability in the Nile flow. Here, this study identifies a region in the southern Indian Ocean with similarly strong teleconnection to the Nile flow. Sea Surface Temperature (SST) in the region (50^oE-80^oE and 25^oS-35^oS) explains 28% of the interannual variability in the Nile flow.
- In addition, four different modes of natural variability in the Nile flow are identified and it is shown that during non-neutral conditions in both the Pacific and Indian Oceans, the Nile flow is highly predictable using global SST information. During those years with anomalous SST conditions in both Oceans, this study estimates that indices of the SSTs in the Pacific and Indian Oceans can collectively explain up to 84% of the interannual

variability in the flow of Nile. The estimated relationships between the Nile flow and these indices allow for accurately predicting the Nile floods and droughts using observed or forecasted conditions of the SSTs in the two oceans.

- This study uses classical Bayesian theorem to develop a new hybrid forecasting algorithm that predicts the Nile flow based on indices of the SST in the Eastern Pacific and Southern Indian Oceans. “Warm” conditions in both oceans translate into 85% probability of “low” flow in the Nile, and insignificant probability of “high” flow. On the other hand, “cold” conditions in both oceans translate into 83% probability of “high” flow in the Nile, and insignificant probability of “low” flow. Applications of the proposed hybrid forecast method should improve predictions of the interannual variability in the Nile flow, adding a new a tool for better management of the water resources of the Nile basin.

The proposed forecasting methodology is indeed dependent on the accuracy of the global SST forecasts from global dynamical models. The accuracy of these forecasts is likely to improve as the models are tested and developed further. However, in this paper we test the proposed forecasting algorithm using observed SSTs. Such test describes an upper limit of the skill of the proposed algorithm. The assessment of the same methodology using indices of SST forecasted by global dynamical models will be addressed in future work.

Tables

Table 1: Summary of the coefficient of determination (R^2) between the average Nile flow from July to October and different combination of indices of ENSO and SIO.

Mode		ENSO	SIO	ENSO, SIO	Number of events (Observed Variance of Nile flow)
ENSO	SIO				
Neutral	Neutral	0.04	0.03	0.08	29 (6.76)
Neutral	Non-Neutral	0.05	0.28^{+}	0.31^{+}	26 (10.24)
Non-Neutral	Neutral	0.4^{+}	0.02	0.43^{+}	26 (5.8)
Non-Neutral	Non-Neutral	0.64^{+}	0.6^{+}	0.84^{+}	19 (12.3)

SIO: South Indian Ocean SSTs index, ENSO: ENSO index.

*Values that are significant at 5% significance level

$^{+}$ Values that are significant at 1% significance level

298

299 **Table 2:** Comparison between regions in the Indian Ocean used in ElDaw et al., 2003 and this
300 study to predict the Nile flow.

Region	Location	Study
1	(35°-44° S, 115° -130° E)	ElDaw et al, 2003
2	(0°-7° S, 90° -130° E)	
3	(35°-44° S, 20° -60° E)	
4	(10°-20° S, 110° -125° E)	
5	(50°E-80°E and 25°S-35°S)	This study

301

302 **Table 3:** Conditional probability of the Nile flow given SIO conditions

		Nile flow		
		High	Normal	Low
SIO	Warm	0	0.25	0.75
	Normal	0.23	0.39	0.39
	Cold	0.57	0.26	0.17

303

304

305 **Table 4:** Conditional probability of the Nile flow given ENSO conditions

		Nile flow		
		High	Normal	Low
ENSO	Warm	0.15	0.31	0.54
	Normal	0.22	0.38	0.41

	Cold	0.68	0.32	0

306

307

308 **Table 5:** Conditional probability of the Nile flow given SIO and ENSO conditions

SIO	Nile flow	ENSO		
		Warm	Normal	Cold
SIO Warm	High	0	0	0
	Normal	0.15	0.22	1
	Low	0.85	0.78	0
SIO Normal	High	0.1	0.14	0.57
	Normal	0.31	0.4	0.43
	Low	0.59	0.46	0
SIO Cold	High	0.33	0.42	0.83
	Normal	0.29	0.33	0.17
	Low	0.37	0.25	0

309

310

311

312

313

314

315

316

317 # Appendix

318 **Table 1:** Summary of some available forecast models of the Sea Surface Temperature

Model	Type of Model	Agency	Domain	Lead time up to (Months)	Resolution (km)	Reference
NCEP-CFS V2	Dynamical	National Centers for Environmental Prediction (NCEP)	Global	8	200	Saha et al., 2010
NASA-GMAO	Dynamical	NASA Goddard Space Flight Center- Global Modeling and Assimilation Office	Global	12	200	Bacmeister et al., 2000
ECMWF-System 4	Dynamical	European Centre for Medium-Range Weather Forecasts	Global	4	70	Molteni et al., 2011
UKMO-GCM	Dynamical	United Kingdom Met Office	Global	6	150	Graham et al., 2005
NOAA-CDC	Statistical	National Oceanic and Atmospheric Administration-Climate Diagnostic Center	Global	12	--	Pneland et al., 1998
CPC-Markov	Statistical	National Centers for Environmental	Nino 3 and Nino 3.4	8	--	Xue et al., 2000

		Prediction-Climate Prediction Center				

REFRENCES

1. Abtew, W., Melesse, A. M. and Dessalegne, T. (2009), El Niño Southern Oscillation link to the Blue Nile River Basin hydrology. Hydrol. Process., 23: 3653–3660. doi: 10.1002/hyp.7367
2. Amarasekera, K. N., Lee, R. F., Williams, E. R., and Eltahir, E. A. B: ENSO and the natural variability in the flow of tropical rivers, J. Hydrol., 200, 24–39, 1996.
3. Beltrando, G., and Camberlin, P., 1993: Interannual variability of rainfall in Eastern Horn of Africa and indicators of atmospheric circulation. International Journal of climatology 13, 533-546.
4. Bacmeister, J. T., P. J. Pegion, S. D. Schubert, and M. J. Suarez, 2000: Atlas of seasonal means simulated by the NSIPP1 atmospheric GCM, NASA Tech. Memo-2000-104606, Vol. 17, 194pp.

5. Black E., J. Slingo, and K.R. Sperber, 2003: An observational study of the relationship between excessively strong short rains in coastal East Africa and Indian Ocean SST. Mon. Wea. Rev., 31, 74-94.

6. Camberlin P., 1995. June-September rainfall in North-Eastern Africa and atmospheric signals over the tropics: a zonal perspective. International Journal of Climatology 15: 773-783.

7. Camberlin, Pierre, 1997: Rainfall Anomalies in the Source Region of the Nile and Their Connection with the Indian Summer Monsoon. J. Climate, 10, 1380–1392.

8. Conway, D., and M. Hulme, 1993: Recent Fluctuations in precipitation and runoff over the Nile subbasins and their impact on Main Nile discharge. Climatic Change, 25, 127 -151.

9. ElDaw, A., J. D. Salas, and L. A. Garcia, 2003: Long Range Forecasting of the Nile River Flows Using Climate Forcing. J. Applied Meteorology, 42:890-904.

10. Eltahir, E. A. B., 1996: ElNino and the natural variability in the flow of the Nile river. Water Resour. Res., 32(1): 131-137.

11. Hastenrath, Stefan, Dierk Polzin, and Charles Mutai, 2011: Circulation Mechanisms of Kenya Rainfall Anomalies. J. Climate, 24, 404–412.

12. Ju, J., and J. M. Slingo, 1995: The Asian summer monsoon and ENSO.Quart. J. Roy. Meteor. Soc., 121, 1133–1168.

13. Kawamura, R., 1998: A possible mechanism of the Asian summer monsoon-ENSO coupling. J. Meteor. Soc. Japan, 76, 1009–1027.

14. Melesse, A., Abtew, W. Setegn, S.G., Desalegn, T. (2011). Hydrological Variability and Climate of the Upper Blue Nile River Basin. In Nile River Basin: Hydrology, Climate and Water Use. Springer. Melesse, Assefa M. (Ed.), 1st Edition., 2011, X, 480 p. 200 illus, Part 1, 3-37, DOI: 10.1007/978-94-007-0689-7_1

15. Molteni, F., T. Stockdale, M. Balmaseda, G. Balsamo, R. Buizza, L. Ferranti, L. Magnusson, K. Mogensen, T. Palmer & F. Vitart, 2011: The new ECMWF seasonal forecast system (System 4). ECMWF Research Department Technical Memorandum n.656, ECMWF, Shinfield Park, Reading RG2-9AX, UK, pp. 51.

16. ElSanabary, M. H., Gan, T. Y., Mwale, D., 204: Application of wavelet empirical orthogonal function analysis to investigate the nonstationary character of Ethiopian rainfall and its teleconnection to nonstationary global Sea Surface Temperature variations for 1900-1998. International Journal of Climatology. DOI:10.1002/joc.3802

17. Graham. R., M. Gordon, P.J. McLean, S. Ineson, M.R. Huddleston, M.K. Davey, A. Brookshaw, R.T.H. Barnes, 2005: A performance comparison of coupled and

uncoupled versions of the Met Office seasonal prediction general circulation model. Tellus, 57A, 320-339.

18. Giro, D. Grimes, D., Black, E. 2011: Teleconnections between Ethiopian summer rainfll and sea surface temperature: part I Observation and Modeling. Climate Dynamics 37:103-199.

19. Gissila, T., Black, E., Grimes, D. I. F., Slingo, J.M 2004: Seasonal forecasting of the Ethiopian Summer rains. International Journal of Climatology 24: 1345-1358.

20. Penland, C. and L. Matrosova, 1998: Prediction of Tropical Atlantic Sea Surface Temperatures Using Linear Inverse Modeling. J. Climate, 11, 483-496.

21. Saha, Suranjana, and Coauthors, 2010: The NCEP Climate Forecast System Reanalysis. Bull. Amer. Meteor. Soc., 91, 1015.1057. doi: 10.1175/2010BAMS3001.1.

22. Suranjana Saha, Shrinivas Moorthi, Xingren Wu, Jiande Wang, Sudhir Nadiga, Patrick Tripp, Hua-Lu Pan, David Behringer, Yu-Tai Hou, Hui-ya Chuang, Mark Iredell, Michael Ek, Jesse Meng, Rongqian Yang, Huug van den Dool, Qin Zhang, Wanqiu Wang, Mingyue Chen, 2013 : The NCEP Climate Forecast System Version 2. (Journal of Climate, under review.)

406 23. Shukla, J., and J. M. Wallace, 1983: Numerical simulation of the atmospheric
407 response to equatorial Pacific sea surface temperature anomalies. J. Atmos. Sci., 40,
408 1613–1630.
409
410 24. Siam, M. S., Wang, G., Estelle, ME., and Eltahir, E. A. B, 2014: Role of the Indian
411 Ocean Sea Surface Temperature in shaping natural variability in the flow of the Nile
412 River. Climate Dynamics, in press.
413
414 25. Soman, M. K., and J. Slingo, 1997: Sensitivity of the Asian summer monsoon to
415 aspects of sea-surface-temperature anomalies in the tropical pacific ocean. Q. J. R.
416 Meteorol. Soc., 123, 309-336.
417
418 26. Trenberth, K. E., 1997: The Definition of El Niño. Bulletin of the American
419 Meteorological Society, 78, 2771-2777.
420
421 27. Wang, G., and Eltahir E. A. B, 1999: Use of ENSO information in Medium and
422 Long Range Forecasting of the Nile Floods . J. Climate, 12, 1726-1737.
423 28. West, M., 1989: Bayesian Forecasting and Dynamic Models. Springer, 704 pp.
424
425
426 29. Winkler, R., 1972: An introduction to Bayesian inference and Decision. Holt,
427 Rinchart and Winstoon, 563 pp.
428

30. Xue, Y., A. Leetmaa, and M. Ji, 2000: ENSO prediction with Markov model: The impact of sea level. J. Climate, 13, 849-871.

31. Yang, J. L., Q. Y. Liu, S. P. Xie, et al., 2007: Impact of the Indian Ocean SST basin mode on the Asian summer monsoon, Geophys. Res. Lett., 34, L02708, doi:10.1029/2006GL028571.

Figures

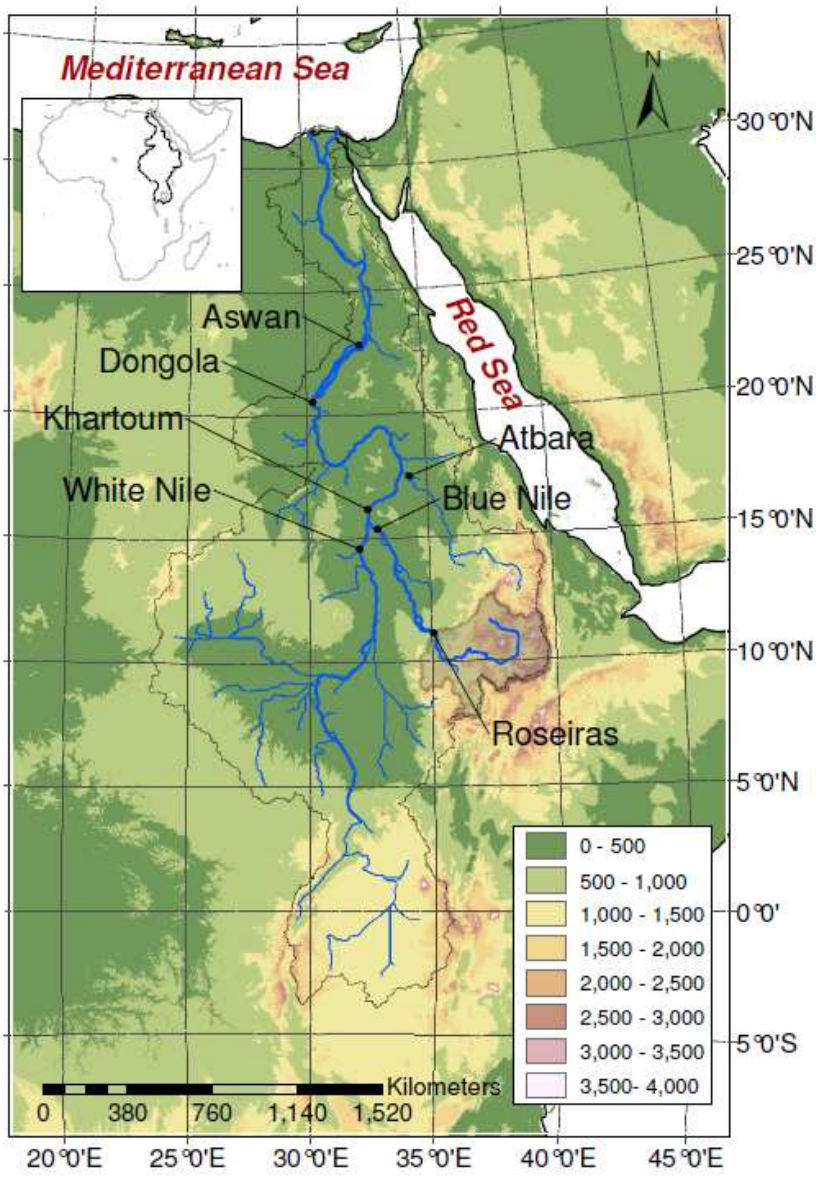
Mediterranean Sea
Red Sea
N
Aswan
Dongola
Khartoum
White Nile
Atbara
Blue Nile
Roseiras
30°0'N
25°0'N
20°0'N
15°0'N
10°0'N
5°0'N
0°0'
5°0'S
0 - 500
500 - 1,000
1,000 - 1,500
1,500 - 2,000
2,000 - 2,500
2,500 - 3,000
3,000 - 3,500
3,500- 4,000
Kilometers
0
380
760
1,140
1,520
20°0'E
25°0'E
30°0'E
35°0'E
40°0'E
45°0'E

Figure 1: Topographic map of the Nile basin showing the outlet of the Upper Blue Nile basin (shaded in gray) at Roseiras. The White and Blue Nile join together at Khartoum the form the main branch of the Nile that flows directly to Dongola in the North.

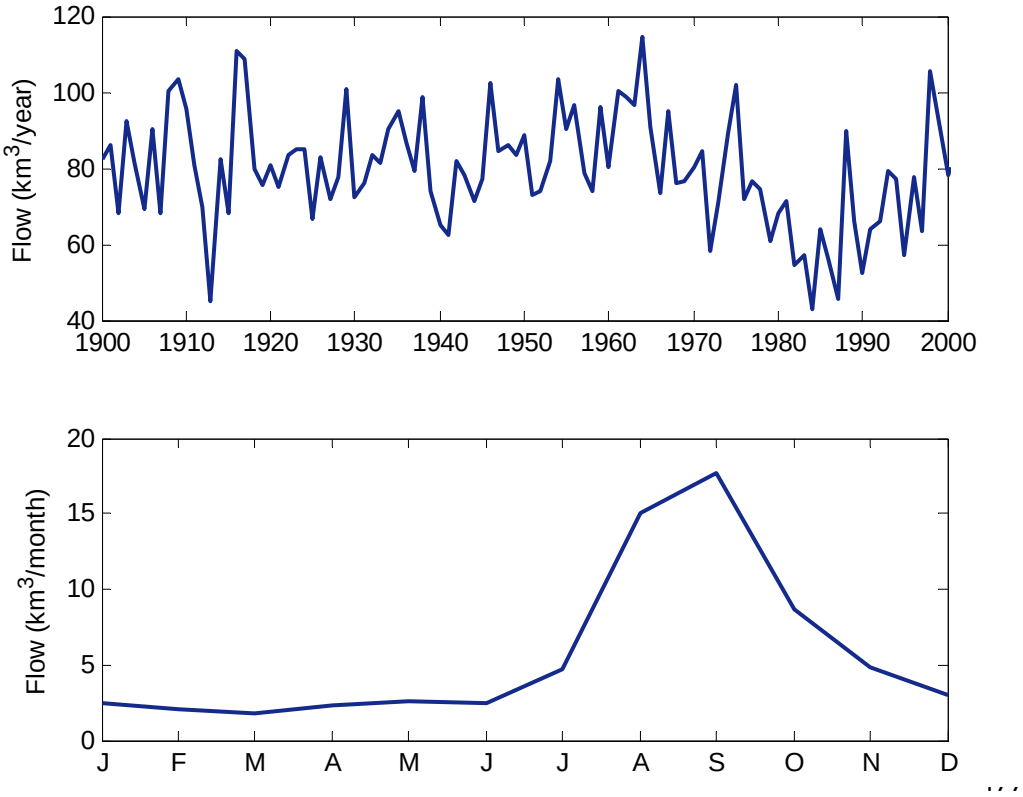

Figure 2: Annual Nile flow (Top) and seasonal cycle (Bottom) of the flow at Dongola for the period from 1900 to 2000.

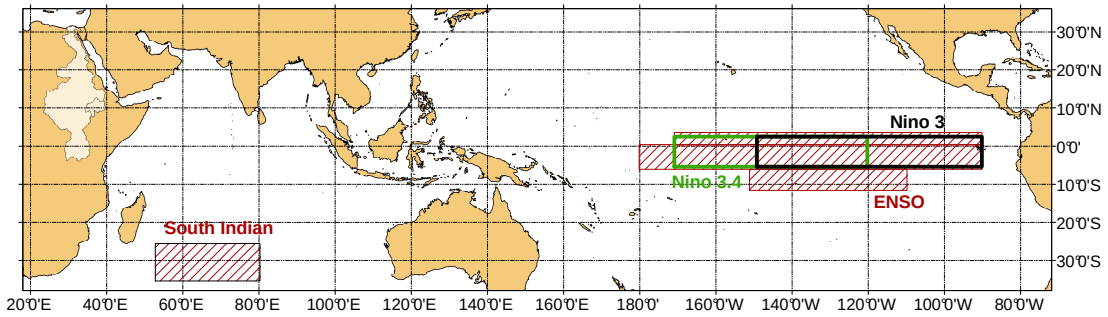

Figure 3: World map showing areas that cover the ENSO and North and South Indian Ocean SSTs indices. The Nino 3 and 3.4 are outlined in blue and green respectively. The whole Nile basin is outlined in black.

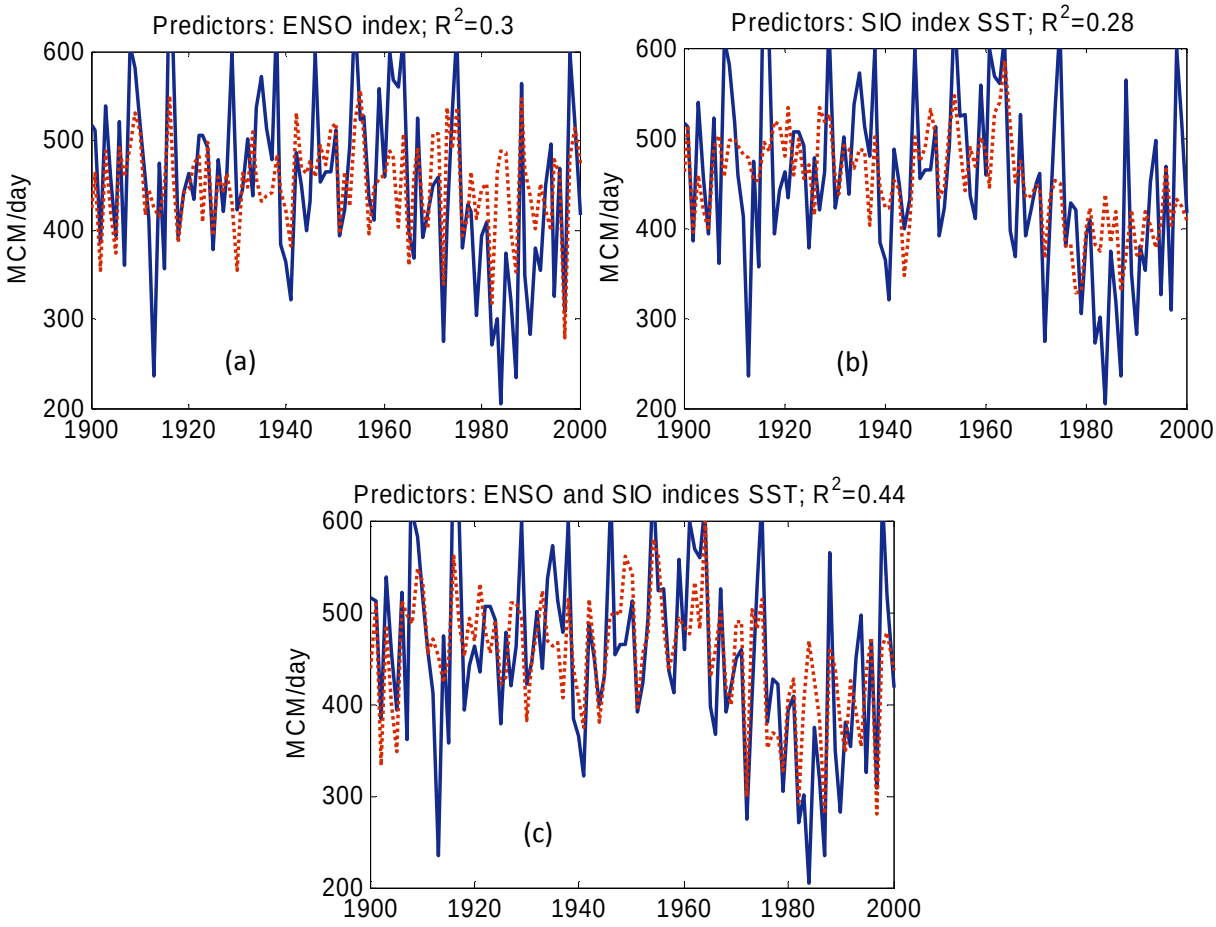

Figure 4: Observed (Solid Blue lines) and simulated (Dashed Red lines) average Nile flows from July to October at Dongola using: a) ENSO index, b) SIO index and c) ENSO and SIO indices as predictors for the period 1900 to 2000.

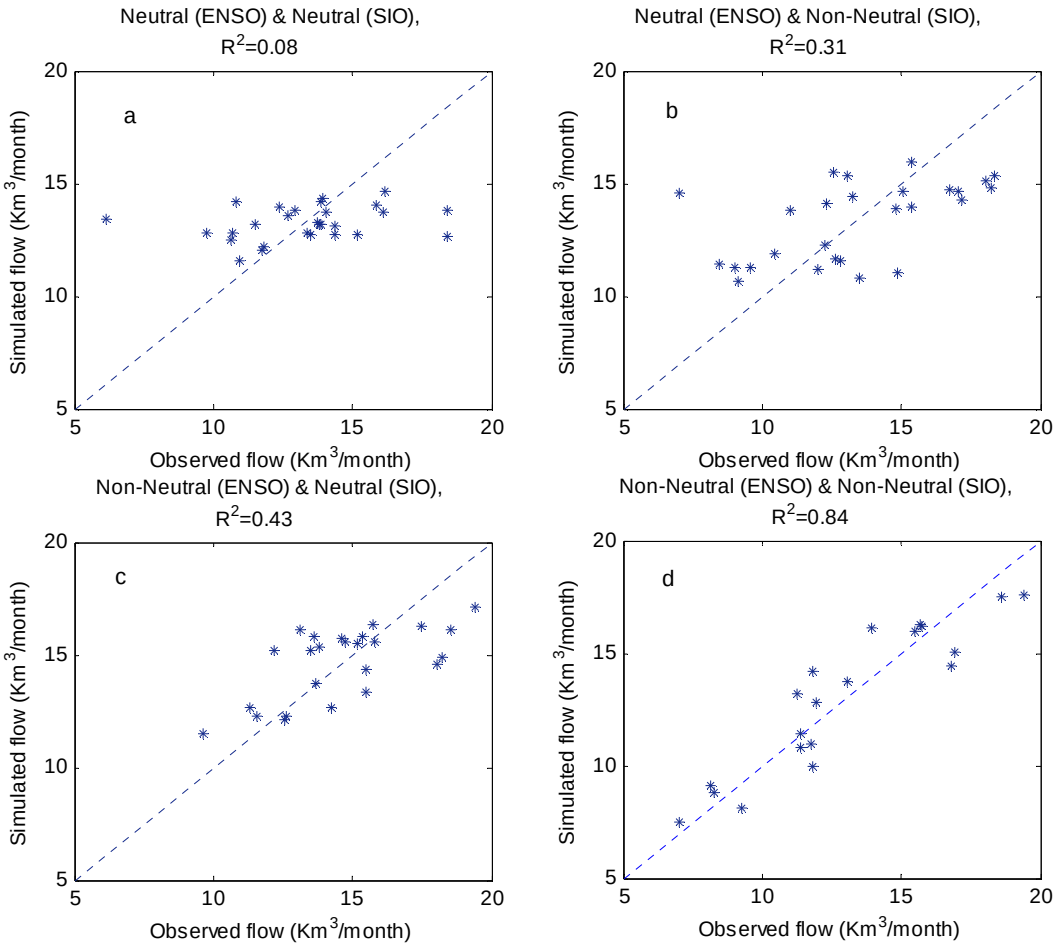

Figure 5: A comparison between the observed and simulated Nile flow showing the different modes of variability for the period from 1900 to 2000: a) Neutral ENSO and SIO, b) Neutral ENSO and Non-Neutral SSTs in SIO, c) Non-Neutral ENSO and Neutral SSTs in SIO and finally, d) Non-Neutral ENSO and Non-Neutral SSTs in SIO.

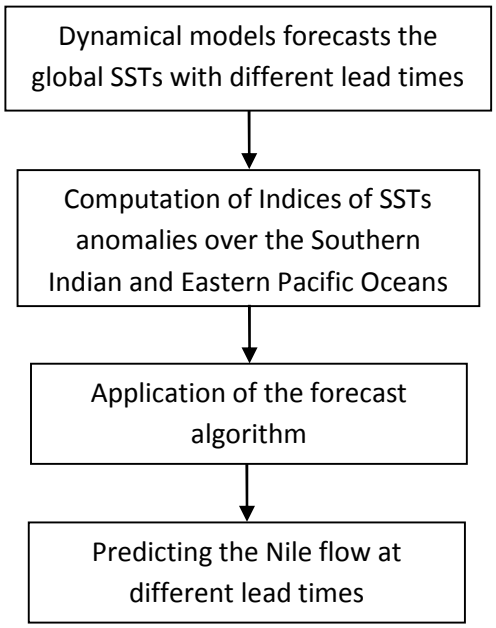

Figure 6: Schematic of the hybrid methodology for predicting the Nile flow using the SSTs forecasts of the dynamical models and the proposed forecast algorithm.

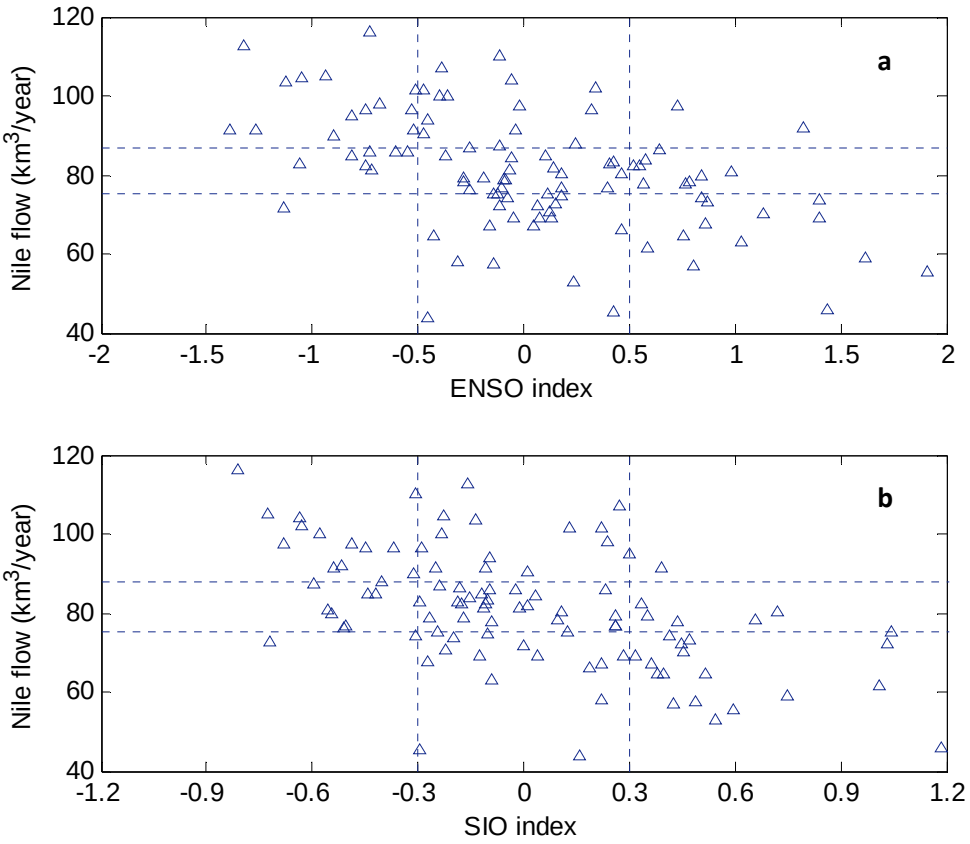

528

529 **Figure 7:** Relations between the annual Nile flow and different indices for the period (1900-2000): a)
530 ENSO, and b) SIO. The horizontal lines represent the boundaries for the “high”, “normal” and “low”
531 categories of the annual flow. The vertical lines represent the boundaries for the “Warm”, “normal”, and
532 “cold” conditions for ENSO and SIO indices.

533

534

535

536

537

538

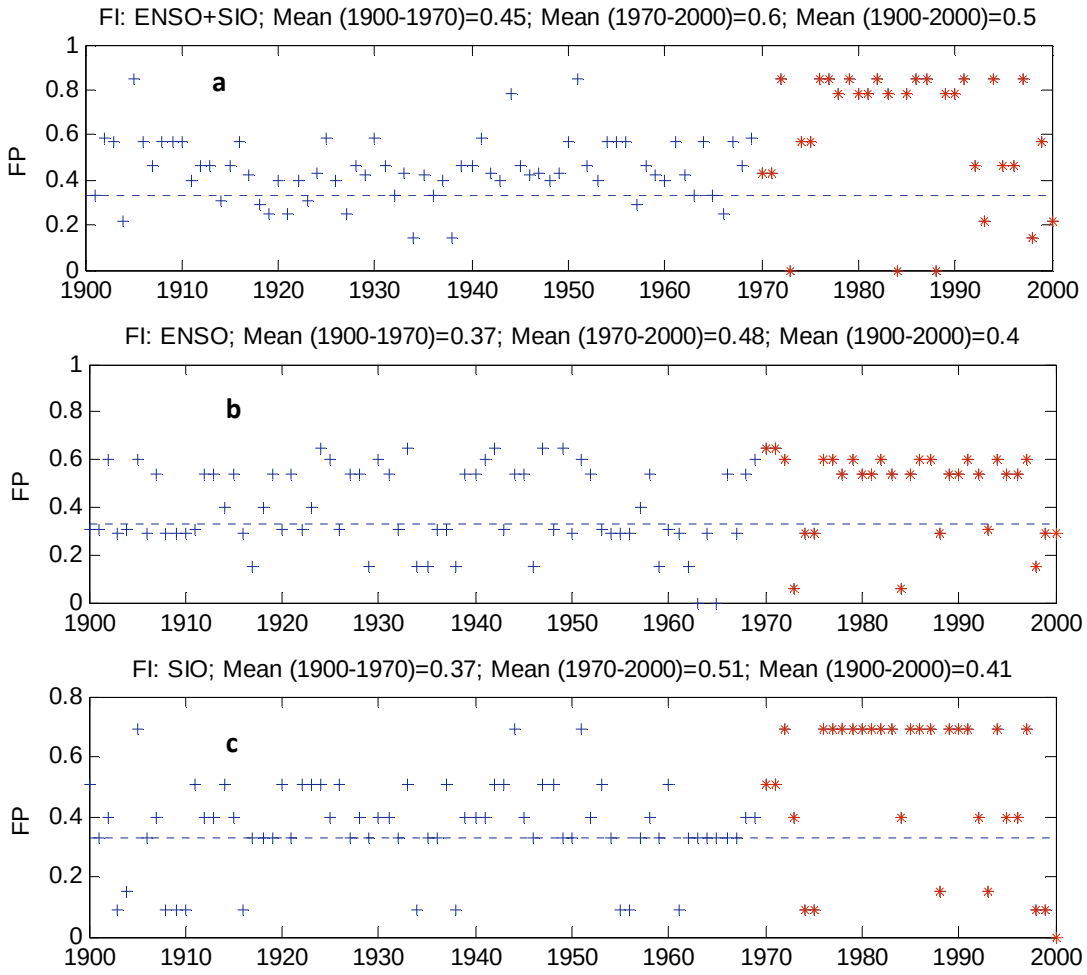

539

540 **Figure 8:** Time series of the forecast probability using different indices: a) ENSO and SIO together, b)
541 ENSO, and c) SIO. The period (1900-1970) is used for calculating the probabilities (shown in crosses)
542 using Eq. (2) and (1970-2000) for validation (shown in stars).

543